Electrochemical Deposition of $Ni(OH)_2$ and Fe-Doped $Ni(OH)_2$ Tubes

Shulei Chou,[a] Fangyi Cheng,[a] and Jun Chen*[a]

Keywords: Nickel hydroxide / Iron doping / Tubes / Electrochemical deposition / Template

Arrays of $Ni(OH)_2$ and Fe-doped $Ni(OH)_2$ tubes were successfully prepared by electrochemical deposition in porous alumina membranes under ambient conditions. Extensive analysis of the tubes was carried out by X-ray diffraction (XRD), scanning electron microscopy (SEM), transmission electron microscopy (TEM) and high-resolution transmission electron microscopy (HRTEM) equipped with energy dispersive spectroscopy (EDS), and X-ray photoelectron spectroscopy (XPS). The results show that the electrodeposition method yielded uniform $Ni(OH)_2$ and Fe-doped $Ni(OH)_2$ tubes with inner diameters of 150–180 nm, wall thicknesses of 20–30 nm, and lengths of about 60 μm. This template-based electrochemical deposition method can be extended to the synthesis of other similar materials such as micro- or nanotubes, -wires, and -rods. Furthermore, the $Ni(OH)_2$ and Fe-doped $Ni(OH)_2$ tubes may have promising applications in alkaline rechargeable batteries and electrocatalytic electrolysis for the production of hydrogen.

Introduction

A variety of 1D nanomaterials including nanotubes, nanorods, nanowires, and nanobelts have become a symbol of the new and fast-developing research area of nanoscience and nanotechnology.[1,2] As members of an important class of 1D nanomaterials, inorganic nanotubes[3–5] such as WS_2,[6] MoS_2,[7] BN,[8] Au,[9] Bi,[10] SiO_2,[11] VO_x,[12] and $NiCl_2$[13] have attracted much attention owing to their special properties. Substantial progress has been achieved in the synthesis of inorganic nanotubes by various methods. For example, the template synthesis,[14–16] in which a template membrane serves as a scaffold for other materials to be assembled with a morphology similar (or complementary) to that of the template pore, is a simple approach to the preparation of inorganic nanotubes such as Au,[9] Si,[17] MoS_2,[18] GaN,[19] and Bi_2O_3.[20]

Nickel hydroxide is the active material in the positive electrodes of alkaline rechargeable batteries such as nickel/cadmium (Ni/Cd), nickel/iron (Ni/Fe), nickel/metal hydride (Ni/MH), and nickel/zinc (Ni/Zn).[21] The capacities of these batteries are usually limited by the positive electrodes for reasons of proper recombination reactions and battery safety. It follows that increasing the energy density of the nickel hydroxide electrode is essential for raising the energy density of such batteries. To improve the characteristics of the nickel hydroxide electrode, much work has been focused on the development of spherical $Ni(OH)_2$ powder and related composite materials.[22–25] On one hand, spherical nickel hydroxide particles exhibit superior electrochemical behavior and higher proton diffusion coefficients.[26,27] On the other hand, the core of the spherical nickel hydroxide powder is still inactive at high-rate and high-temperature charge/discharge because of the diffusion barrier, which can be improved by using $Ni(OH)_2$ tubes.[28]

Electrolysis is an attractive process for hydrogen production from alkaline solutions when cheap solar power is available. A potentially more important application of Fe-doped $Ni(OH)_2$ tubes is their use as oxygen-evolving anodes for the electrolytic production of hydrogen. This is due to their low overpotential and stability in alkaline solution.[29] The tubelike Fe-doped $Ni(OH)_2$, which has a high specific surface area, could be very useful in hydrogen production in the future.

Electrochemical deposition, which is a convenient method to control the thickness of the deposited product, has already been used to prepare $Ni(OH)_2$ and Fe-doped $Ni(OH)_2$ thin films for a few years.[30–32] Four possible mechanisms of electrochemical deposition of $Ni(OH)_2$ from nickel nitrate solution have been proposed by MacArthur.[33] Furthermore, electrochemical deposition in Al_2O_3 templates has recently been used to prepare inorganic micro- or nanotubes of Au,[34] Co, Fe,[35] Ni,[36] Cu,[37] Pt,[38] CdS,[39] and TiO_2.[40] The process of electrochemical deposition of metal nanotubes under low-current-density conditions occurs by simultaneous deposition along the holes of the membranes.[41] However, to the best of our knowledge, the synthesis of metal hydroxide tubes or nanotubes by electrochemical deposition in templates is limited.

Here we report on the preparation of $Ni(OH)_2$ and Fe-doped $Ni(OH)_2$ tubes by electrochemical deposition in the pores of alumina membranes. The results show that the wall

[a] Institute of New Energy Material Chemistry, Nankai University,
Tianjin 300071, P.R. China
E-mail: chenabc@nankai.edu.cn

thickness of the $Ni(OH)_2$ and Fe-doped $Ni(OH)_2$ tubes is easily controlled by adjusting the reaction conditions. This method can be extended to the synthesis of other similar micro- or nanotubes, -wires, and -rods.

Results and Discussion

Figure 1 shows the XRD patterns of the α-$Ni(OH)_2$ (Figure 1a) and Fe-doped α-$Ni(OH)_2$ tubes (Figure 1b). The peaks in Figure 1a can be indexed as a hexagonal structure of α-$Ni(OH)_2$·$0.75H_2O$ with the lattice parameters a = 3.08 Å and c = 23.41 Å, which are in good agreement with the standard value (ICDD-JCPDS card 38–0715). The broadening of the peaks in the XRD pattern indicates that the product consists of nanocrystallites, in which amorphous particles may coexist. Figure 1b shows the XRD pattern of Fe-doped α-$Ni(OH)_2$ tubes. The 2θ value of each peak is in accordance with α-$Ni(OH)_2$·$0.75H_2O$ as shown in Figure 1a. However, the relative intensities of the peaks at 11.70° and 23.58° in Figure 1b are higher than those in Figure 1a. This might arise from the Fe-doping. That is, the incorporation of Fe in the Ni lattice sites of α-$Ni(OH)_2$ might have caused the intensity changes. Therefore, a further investigation by XPS was used to verify the existence and form of Fe present.

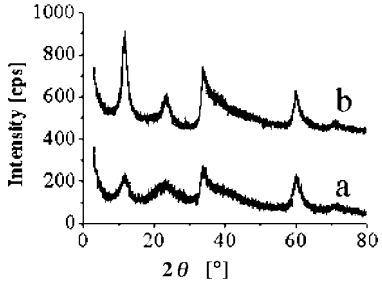

Figure 1. X-ray diffraction patterns of the α-$Ni(OH)_2$ tubes (a) and Fe-doped α-$Ni(OH)_2$ tubes (b).

Figure 2 shows the XPS spectra of the Fe-doped α-$Ni(OH)_2$ tubes. Figure 2a shows that the sample contains Fe, Ni and O. Figure 2b shows that a binding energy of 855.8 eV is assigned to Ni $2p_{3/2}$ in $Ni(OH)_2$. Figure 2c shows the Fe 2p spectrum of the tubes produced. The Fe-doped $Ni(OH)_2$ tubes contain only Fe^{III} because two binding energies of 725.3 eV and 711.1 eV were detected, which are assigned to Fe $2p_{1/2}$ and Fe $2p_{3/2}$ in Fe_2O_3, respectively.[42] Balasubramanian et al.[32] reported that cathodic codeposition of Fe^{II} with Ni^{II} led to the incorporation of Fe in the Ni lattice sites of α-$Ni(OH)_2$ and these Fe ions were present as Fe^{III}. Our XPS and XRD studies have confirmed this report and have shown that the Fe-doped $Ni(OH)_2$ tubes are Fe^{III}-doped α-$Ni(OH)_2$·$0.75H_2O$. The quantitative XPS study of Fe-doped $Ni(OH)_2$ tubes shows that the atomic ratio of Fe to Ni is 1:3.7. Since Corrigan's study shows that iron/nickel hydrous oxides with this atomic ratio are very useful in lowering the Tafel slope for catalyzing the oxygen evolution reaction,[29] we believe that the Fe^{III}-doped α-$Ni(OH)_2$·$0.75H_2O$ tubes have potential uses as electrocatalysts for alkaline electrolysis to produce hydrogen.

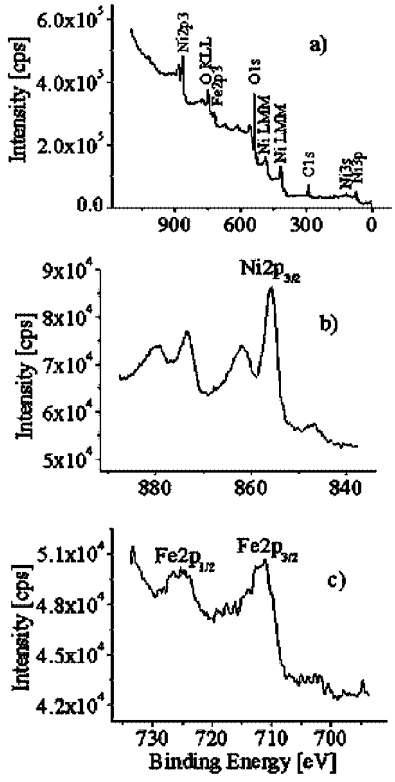

Figure 2. XPS spectra of Fe-doped $Ni(OH)_2$ tubes in the binding energy range of (a) 0–1100 eV, (b) 840–890 eV, and (c) 695–735 eV.

Figure 3 shows the SEM images of the $Ni(OH)_2$ (Figure 3a–c) and Fe-doped $Ni(OH)_2$ tubes (Figure 3d and e) at different magnifications. Figure 3a is an overall view of the $Ni(OH)_2$ tubes, which shows that bundles of standing or lying $Ni(OH)_2$ tubes were obtained. The length of the $Ni(OH)_2$ tube bundles is approximately 60 μm, which corresponds to the thickness of the template membrane employed in the synthetic process. In Figure 3a shorter and broken bundles can also be found, which may arise from the weakness of the tubes. Figure 3b shows that the $Ni(OH)_2$ tubes are arranged roughly parallel to one another with a smooth-surface alignment. This might be due to a remaining trace of the alumina matrix rather than any kind of self-organization. Figure 3c is the high-magnification SEM image of the bundle tips of the $Ni(OH)_2$ tubes which shows their open-ended character. The $Ni(OH)_2$ tubes are cylinders with a wall thickness of 20–30 nm. There is a distribution of diameters of the tubes around 200 nm because of the pore-diameter distribution of the template. Figure 3d and Figure 3e show the SEM images of Fe-doped $Ni(OH)_2$ tubes at different magnifications. Figure 3d shows a bundle of Fe-doped $Ni(OH)_2$ tubes, which is not as uniform as the $Ni(OH)_2$ tubes. Figure 3e, which is the enlargement of the square marked in Figure 3d, shows a clear view of the Fe-doped $Ni(OH)_2$ tubes with open-ended tips. It should be noted that when we removed Fe-doped $Ni(OH)_2$ tubes from the alumina membranes, almost all of them were broken.

Thus, the Fe-doped $Ni(OH)_2$ tubes are not as long as the $Ni(OH)_2$ tubes. This may be due to the Fe doping.

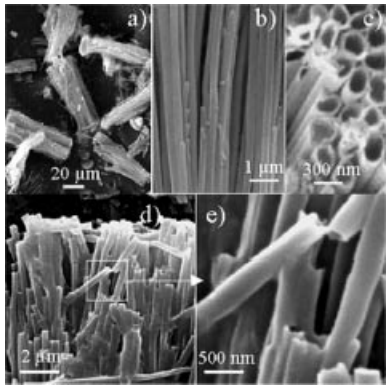

Figure 3. Typical SEM images of the $Ni(OH)_2$ (a, b, c) and Fe-doped $Ni(OH)_2$ tubes (d, e). $Ni(OH)_2$ tubes: (a) overall view, (b) walls of the tube bundles, and (c) tube bundle tips at high magnification. Fe-doped $Ni(OH)_2$ tubes: (d) low magnification and (e) enlargement of the square marked in (d).

To understand the structure in further detail, the $Ni(OH)_2$ and Fe-doped $Ni(OH)_2$ tubes were inspected with TEM (Figure 4). Figure 4a shows the TEM image of the $Ni(OH)_2$ tubes at a lower magnification. In addition to the tubes there are some particles in the product. This phenomenon arises from the strong supersonic vibrations used in the sample preparation for TEM analysis, that is, some of the tubes were broken down into shorter ones and then into particles. Figure 4b shows a TEM image of an open-ended $Ni(OH)_2$ tube. The centers of the mesostructures are bright in contrast to their edges, confirming their hollow-tube nature. The inner diameters are about 150–160 nm, and the wall thickness is about 20–30 nm. Figure 4c shows the TEM image of the tube wall. It can be seen that the surface of the tube is smooth with an amorphous structure. This is consistent with the XRD analysis. Figure 4d shows that most of the Fe-doped $Ni(OH)_2$ tubes have similar wall thickness, and there is also an interesting branchlike structure which simply reflects the structure of alumina templates. That is, the template contains not only aligned pores but also some abnormal structures that look like branches. This phenomenon also means that, if we have the template, we can also prepare some complex tubular structures by this method. A view of the open-ended Fe-doped $Ni(OH)_2$ tubes is shown in Figure 4e, from which we can estimate that the tubes have an inner diameter of about 170–180 nm. EDS analysis in Figure 5 shows that the tubes in Figure 4e contain three elements, Fe, Ni, and O, and two other elements, Cu and C, which come from the carbon-coated copper grid. This is consistent with the XRD and XPS studies. The TEM image in Figure 4f shows that the Fe-doped $Ni(OH)_2$ tubes are needlelike structures with wall thicknesses of about 20–30 nm. The needlelike structure of Fe-doped $Ni(OH)_2$ tubes is weaker than the smooth-surface structure of $Ni(OH)_2$ tubes, so it might not be easy to prepare long bundles of Fe-doped $Ni(OH)_2$ tubes like the $Ni(OH)_2$ tubes under the same conditions.

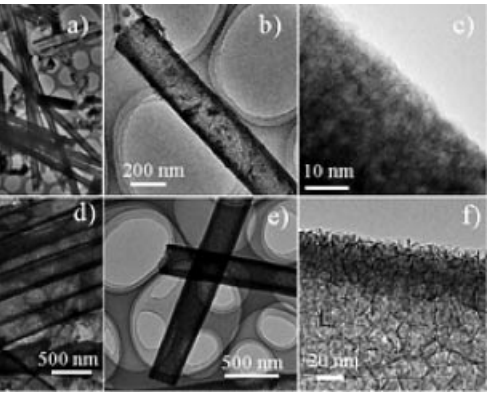

Figure 4. Representative TEM images of the $Ni(OH)_2$ (a, b, c) and Fe-doped $Ni(OH)_2$ tubes (d,e,f).

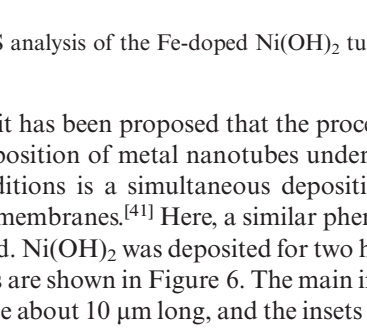

Figure 5. EDS analysis of the Fe-doped $Ni(OH)_2$ tubes taken from Figure 4e.

Recently, it has been proposed that the process of electrochemical deposition of metal nanotubes under low-current-density conditions is a simultaneous deposition along the holes of the membranes.[41] Here, a similar phenomenon was also observed. $Ni(OH)_2$ was deposited for two hours, and the TEM images are shown in Figure 6. The main image shows a $Ni(OH)_2$ tube about 10 μm long, and the insets (a, b, c and d) are the corresponding magnifications marked on the tube. The wall thickness of the $Ni(OH)_2$ tubes are different on the Au side of the membrane. It can be clearly seen from Figure 6 that the wall thickness decreases from Figure 6d to Figure 6a. This is especially evident as shown in Figure 6d where the

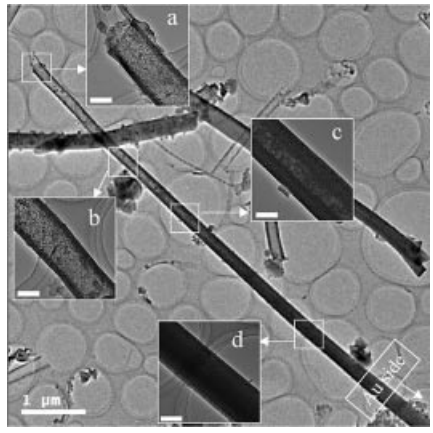

Figure 6. TEM images of $Ni(OH)_2$ deposited in the template for 2 h. The insets (a, b, c, and d) are the corresponding magnifications marked on the tube. Scale bars in the insets represent 100 nm.

tubes are already completely filled. Therefore, when we use electrochemical deposition in templates to prepare tubular semiconductors, attention must be paid to control the deposition time. Depositing for quite a long time such as 10 h leads to wire- or rodlike semiconductors. Figure 7 shows the TEM images of $Ni(OH)_2$ rods which were deposited for 10 h. Figure 7a shows several $Ni(OH)_2$ rods which are about 6 μm long and about 200 nm in outer diameter. Figure 7b shows the smooth-surface structure which is consistent with the structure of the $Ni(OH)_2$ tubes above.

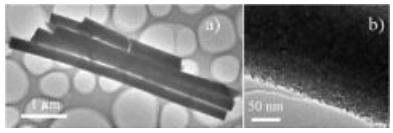

Figure 7. TEM images of the $Ni(OH)_2$ rods prepared by electrochemical deposition for 10 hours at low (a) and high (b) magnification.

Conclusions

Arrays of α-$Ni(OH)_2 \cdot 0.75H_2O$ and Fe^{III}-doped α-$Ni(OH)_2 \cdot 0.75H_2O$ tubes were prepared by electrochemical deposition in porous alumina membranes. The smooth-surface α-$Ni(OH)_2 \cdot 0.75H_2O$ tubes are more uniform and stronger than the needlelike Fe-doped α-$Ni(OH)_2 \cdot 0.75H_2O$ tubes. Nanostructures of tubes to wires or rods can be obtained by controlling the depositing conditions. It is obvious that this method of template-based electrochemical deposition can be extended for the synthesis of other similar materials such as micro- or nanotubes, -wires, and -rods.

Experimental Section

Electrochemical Deposition: A thin Au layer was evaporated onto one side of the pore walls of the alumina membranes (Whatman, Φ47 mm with 0.2-μm pores and 60 μm thickness), which was used as the working electrode for the electrochemical deposition. The Au-coated side of the alumina membrane was pasted on a Ni sheet with electric adhesive tape and the rest of the Ni tape was covered with insulated adhesive tape. The face and the side of the working electrode are schematically shown in Figure 8. The counter electrode was a nickel plate about 1.0 cm^2. The conditions for the electrochemical deposition of pure $Ni(OH)_2$ tubes and Fe-doped $Ni(OH)_2$ tubes are summarized in Table 1. Before the electrochemical deposition, the working electrode was submerged in the electrolyte, which was stirred by an electromagnetic blender, for 2 hours in order to make the electrolyte penetrate into the membranes. The electrochemical deposition was done in a plating bath under constant current and controlled temperature.

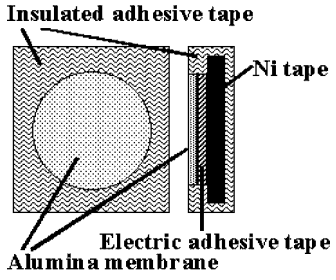

Figure 8. Schematic diagram showing the working electrode for electrochemical deposition of pure $Ni(OH)_2$ and Fe-doped $Ni(OH)_2$ tubes.

Table 1. The electrochemical deposition conditions for preparing pure $Ni(OH)_2$ and Fe-doped $Ni(OH)_2$ tubes.

Tubes	Electrolyte composition	Temp. (°C)	Curr. dens. ($mA\,cm^{-2}$)	Time (min)
$Ni(OH)_2$	0.05 M $Ni(NO_3)_2 \cdot 6H_2O$	20	10	10
Fe-doped $Ni(OH)_2$	0.05 M $Ni(NO_3)_2 \cdot 6H_2O$	20	5	20
	0.001 M $Fe(NH_4)_2(SO_4)_2 \cdot 6H_2O$			

Instrumental Analyses: The alumina membranes with the prepared samples were peeled off the Ni tape and immersed in 2 M NaOH for 4 h to remove the alumina template. After careful rinsing with deionized water, the samples were characterized using a combination of the following techniques: XRD, SEM, TEM and HRTEM equipped with EDS, and XPS.

XRD analysis was carried out with a Rigaku INT-2000 X-ray generator. The X-ray intensity was measured over a diffraction 2θ angle from 3° to 80° with a velocity of 0.02°/step and 2°/min. Specimens for SEM were collected on an electric adhesive tape and allowed to air-dry before the measurement. The electric adhesive tape with the sample was fixed to a piece of glass, which was attached to a SEM stub and then sputtered with a 2-nm layer of gold. Images were taken with a Philips XL-30 scanning electron microscope working at an accelerating voltage of 20 kV. Samples for TEM were put into an alcohol-water sonicator for about 5 min. Then the samples were collected on a carbon-coated copper grid and allowed to air-dry before the measurement. Images were obtained with a Philips Tecnai F20 TEM working at an accelerating voltage of 200 kV. EDS was performed in the microscope with use of a Kevex Super 8000 detector. The composition of the Fe-doped $Ni(OH)_2$ tubes was examined with an XPS (ESCA-3400, Shimadzu Electron) using monochromatic Mg–K_α radiation (1253.6 eV). The binding energy values were referenced to the carbon C 1*s* core peak at 284.7 eV.

Acknowledgments

This work was supported by the NSFC (20325102 and 90406001) and MoE (104055 and 2004164).

[1] T. Braun, A. P. Schubert, R. N. Kostoff, *Chem. Rev.* **2000**, *100*, 23–37.
[2] L. Hueso, N. Mathur, *Nature* **2004**, *427*, 301–304.
[3] C. N. R. Rao, M. Nath, *Dalton Trans.* **2003**, 1–24.
[4] a) G. R. Patzke, F. Krumeich, R. Nesper, *Angew. Chem. Int. Ed.* **2002**, *41*, 2446–2461; b) R. Tenne, *Angew. Chem. Int. Ed.* **2003**, *42*, 5124–5132.
[5] M. Remskar, *Adv. Mater.* **2004**, *16*, 1497–1504.
[6] R. Tenne, L. Margulis, M. Genut, G. Hodes, *Nature* **1992**, *360*, 444–446.
[7] Y. Feldman, E. Wasserman, D. J. Srolovitz, T. Tenne, *Science* **1995**, *267*, 222–225.
[8] N. G. Chopra, R. G. Luyken, K. Cherrey, V. H. Crespi, M. L. Cohen, S. G. Louie, A. Zettl, *Science* **1995**, *269*, 966–967.
[9] J. C. Hutleen, K. B. Jirage, C. R. Martin, *J. Am. Chem. Soc.* **1998**, *120*, 6603–6604.
[10] a) Y. D. Li, J. W. Wang, Z. X. Deng, Y. Y. Wu, X. M. Sun, D. P. Yu, P. D. Yang, *J. Am. Chem. Soc.* **2001**, *123*, 9904–9905; b) B. Yang, C. Li, H. Hu, X. Yang, Q. Li, Y. T. Qian, *Eur. J. Inorg. Chem.* **2003**, 3699–3702.

[11] H. Nakamura, Y. Matsui, *J. Am. Chem. Soc.* **1995**, *117*, 2651–2652.
[12] M. E. Spahr, P. Bitterli, R. Nesper, M. Muller, F. Krumeich, H. U. Nissen, *Angew. Chem. Int. Ed.* **1998**, *37*, 1263–1265.
[13] Y. R. Hacohen, E. Grunbaum, R. Tenne, J. Sloan, J. L. Hutchison, *Nature* **1998**, *395*, 336–337.
[14] C. R. Martin, *Science* **1994**, *266*, 1961–1966.
[15] F. Schuth, *Angew. Chem. Int. Ed.* **2003**, *42*, 3604–3622.
[16] K. J. C. van Bommel, A. Friggeri, S. Shinkai, *Angew. Chem. Int. Ed.* **2003**, *42*, 980–999.
[17] J. Sha, J. Niu, X. Ma, J. Xu, X. Zhang, D. Yang, *Adv. Mater.* **2002**, *14*, 1219–1221.
[18] C. M. Zelenski, P. K. Dorhout, *J. Am. Chem. Soc.* **1998**, *120*, 734–742.
[19] J. Goldberger, R. He, Y. Zhang, S. Lee, H. Yan, H. J. Choi, P. Yang, *Nature* **2003**, *422*, 599–602.
[20] B. Yang, M. Mo, H. Hu, C. Li, X. Yang, Q. Li, Y. T. Qian, *Eur. J. Inorg. Chem.* **2004**, 1785–1787.
[21] D. Linden, *Handbook of Batteries*, 3rd ed., McGraw-Hill, New York, **2002**.
[22] M. Oshitani, M. Watada, T. Tanaka, T. Iida, in *Hydrogen and Metal Hydride Batteries*, vol. 94 (Eds.: P. D. Bennett, T. Sakai), The Electrochemistry Society, Pennington, NJ, **1994**, p. 303.
[23] B. Liu, X. Y. Wang, H. T. Yuan, Y. S. Zhang, D. Y. Song, Z. X. Zhou, *J. Appl. Electrochem.* **1999**, *29*, 855–860.
[24] M. Fojas, E. Murphy, P. Stroeve, *Ind. Eng. Chem. Res.* **2002**, *41*, 2662–2667.
[25] I. Zhitomirsky, *J. Appl. Electrochem.* **2004**, *34*, 235–240.
[26] E. David, J. Alvin, R. Peter, T. Xiao, *J. Power Sources* **1997**, *65*, 231–233.
[27] X. Wang, H. Luo, P. V. Parkhutik, A. C. Millan, E. Matveeva, *J. Power Sources* **2003**, *115*, 153–160.
[28] F. S. Cai, G. Y. Zhang, J. Chen, X. L. Gou, H. K. Liu, S. X. Dou, *Angew. Chem. Int. Ed.* **2004**, *43*, 4212–4216.
[29] A. Corrigan, *J. Electrochem. Soc.* **1987**, *134*, 377–384.
[30] H. Bode, K. Dehmelt, J. Witte, *Electrochim. Acta* **1966**, *11*, 1079–1087.
[31] Oliva, J. Leonardi, J. F. Laurent, *J. Power Sources* **1982**, *8*, 229–255.
[32] M. Balasubramanian, C. A. Melendres, S. Mini, *J. Phys. Chem. B* **2000**, *104*, 4300–4306.
[33] D. M. MacArthur, *J. Electrochem. Soc.* **1970**, *117*, 422–425.
[34] C. J. Brumlik, C. R. Martin, *J. Am. Chem. Soc.* **1991**, *113*, 3174–3175.
[35] G. Tourillon, L. Pontonnier, J. P. Levy, V. Langlais, *Electrochem. Solid-State Lett.* **2000**, *3*, 20–23.
[36] J. Bao, C. Tie, Z. Xu, Q. Zhou, D. Shen, Q. Ma, *Adv. Mater.* **2001**, *13*, 1631–1633.
[37] Y. H. Wang, C. H. Ye, X. S. Fang, L. D. Zhang, *Chem. Lett.* **2004**, *33*, 166–167.
[38] Y. Zhao, Y. G. Guo, Y. L. Zhang, K. Jiao, *Phys. Chem. Chem. Phys.* **2004**, *6*, 1766–1768.
[39] S. M. Zhou, Y. S. Feng, L. D. Zhang, *Eur. J. Inorg. Chem.* **2003**, 1794–1797.
[40] P. Hoyer, *Langmuir* **1996**, *12*, 1411–1413.
[41] W. C. Yoo, J. K. Lee, *Adv. Mater.* **2004**, *16*, 1097–1101.
[42] J. F. Moulder, W. F. Stickle, P. E. Sobol, K. D. Bomben, in *Handbook of X-ray Photoelectron Spectroscopy* (Ed.: J. Chastain), Perkin–Elmer Corporation, Wellesley, MA, **1992**.

Received: January 25, 2005
Published Online: September 9, 2005

